

## On $\gamma$ rays as predictors of UHECR flux in AGNs

CAINÃ DE OLIVEIRA,<sup>1</sup> RODRIGO GUEDES LANG,<sup>2</sup> AND PEDRO BATISTA<sup>2</sup>

<sup>1</sup>*Instituto de Física de São Carlos, Universidade de São Paulo, Av. Trabalhador São-carlense 400, São Carlos, Brasil.*

<sup>2</sup>*Friedrich-Alexander-Universität Erlangen-Nürnberg, Erlangen Centre for Astroparticle Physics, Nikolaus-Fiebiger-Str. 2, 91058 Erlangen, Germany*

(Dated: August 22, 2024)

### ABSTRACT

Active galactic nuclei (AGN) are among the main candidates for ultra-high-energy cosmic ray (UHECR) sources. However, while theoretical and some phenomenological works favor AGNs as the main sources, recent works have shown that using the very-high-energy (VHE)  $\gamma$ -ray flux as a proxy for the UHECR flux leads to a bad agreement with data. In this context, the energy spectrum and composition data are hardly fitted. At the same time, the arrival directions map is badly described and a spurious dipole direction is produced. In this work, we propose a possible solution to these contradictions. Using the observed  $\gamma$ -ray flux as a proxy may carry the implicit assumption of beamed UHECR emission and, consequently, its beam will remain collimated up to its detection on Earth. We show that assuming an isotropic UHECR emission and correcting the  $\gamma$ -ray emission proxy by Doppler boosting can overcome the problem. The combined fit of the spectrum and composition is improved by  $3.56\sigma$ , while the predicted arrival directions agree much better with the data. In particular, a spurious direction of the dipole can be reduced from  $10.3$  ( $5.4$ ) $\sigma$  away from the data to  $2.2$  ( $1.5$ ) $\sigma$  for  $E > 8$  EeV ( $E > 32$  EeV). We also show that this effect is particularly important when including AGNs of different classes in the same analysis, such as radio galaxies and blazars.

### 1. INTRODUCTION

The first detection of ultra-high energy cosmic rays (UHECRs) (Linsley 1963) raised significant questions about their origin. The discovery of astrophysical objects responsible for the acceleration of particles to ultra-high energies remains one of the most compelling mysteries in contemporary science (Kotera & Olinto 2011; Alves Batista et al. 2019). The small flux of UHECRs requires experiments with a very large area, up to thousands of square kilometers, to improve the detection of events and minimize experimental uncertainties (Nagano & Watson 2000). The Pierre Auger Observatory (The Pierre Auger Collaboration 2015) and Telescope Array (Abu-Zayyad et al. 2012) are the best examples of such feat with unprecedented exposure, leading to large statistics of high-quality data that allowed precision studies in the ultra-high-energy range.

UHECR arrival direction measurements have been extensively used in the search for UHECR accelerators. On the large-scale anisotropies, one of the most significant results comes in the form of the dipole measured by the Pierre Auger Observatory. The measured dipole reaches  $5.2\sigma$  confidence level (CL) for events with energies greater than 8 EeV and points outward the galactic center at ( $\alpha = (100 \pm 10)^\circ$ ,  $\delta = (-24_{-13}^{+12})^\circ$ ), which is powerful evidence for the dominance of extragalactic UHECR above this energy (The Pierre Auger Collaboration et al. 2017). For small-scale anisotropies, Abreu et al. (2022) reported a correlation between the arrival direction data of events with energies greater than 39 EeV and a jetted active galactic nuclei (AGN) catalog with a confidence of  $3.3\sigma$ . The same analysis performed with a starburst galaxy (SBG) catalog reached  $4.2\sigma$  confidence level. Combining Pierre Auger and Telescope Array data, a full-sky search for sources showed a correlation of  $4.7\sigma$  ( $> 38/49$  EeV for Auger/TA) with the SBG catalogue (di Matteo, A. et al. for the Pierre Auger and Telescope Array collaborations 2023).

caina.oliveira@usp.br

rodrigo.lang@fau.de

pedro.batista@fau.de

To consider particle physics processes and cosmic magnetic field deflections involved during the travel from the source to Earth, Monte Carlo simulations have been developed (Batista et al. 2016; Aloisio et al. 2017). The results of numerical propagation are compared with observations, and the free parameters of the model (nuclei fraction, spectral index, maximum energy, spectrum normalization) are constrained by fitting the simulation results to experimental data (see, for example, Aab et al. (2017); Eichmann et al. (2022); Abdul Halim et al. (2024)).

Although the acceleration mechanism is generally assumed to be identical for a given class of objects (i.e., assuming identical spectral index), different approaches have been used to predict the UHECR luminosity of each object (Aab et al. 2018a; Eichmann et al. 2018; Eichmann 2019; Eichmann et al. 2022; Abreu et al. 2022; de Oliveira & de Souza 2022, 2023; Abdul Halim et al. 2024; Partenheimer et al. 2024).

Several works investigate AGNs as possible sources of UHECR. They differ in their assumption about the normalization of the UHECR flux from each source. While some assumptions lead to good agreement with the experimental data (Eichmann et al. 2018; Eichmann 2019; Eichmann et al. 2022; de Oliveira & de Souza 2022, 2023), this is not the case when the  $\gamma$ -ray luminosity ( $L_\gamma$ ) is used as a proxy for the UHECR luminosity ( $L_{CR}$ ) (Abdul Halim et al. 2024; Partenheimer et al. 2024). In this case, the main issue is that the strong signal from the jetted AGN Mkn 421 ( $\sim 130$  Mpc) generates a fortuitous hotspot and dominates the dipole direction. In addition, the fit to the spectrum is worsened by the high contribution of distant sources.

In this work, we propose a possible way to conciliate these two views by reviewing the motivations behind the use of  $L_\gamma$  as a proxy for  $L_{CR}$ . In section 2 we present a comparison of the theoretical predictions for the acceleration of UHECRs in AGN jets and the origin of the  $\gamma$ -ray radiation. We show that  $L_\gamma$  should be used carefully when used as a weight to the UHECR flux. In section 3 it is shown that, when considering the intrinsic  $\gamma$ -ray luminosity rather than the observed  $\gamma$ -ray luminosity, the combined fit of the spectrum and composition data is slightly improved, while the agreement between the predicted arrival directions and data vastly improves. The main results and outlook of this work are summarized in section 4.

## 2. REVIEWING GAMMA RAYS AND CRS IN JETS

The deflections suffered by cosmic rays during the trajectory from the accelerator to the detection prevent the direct identification of its sources. Without reliable models of the extragalactic and galactic magnetic fields, theoretical arguments are combined with constraints of cosmic magnetic fields in the source search. The usual approach for investigating possible individual sources focuses on the so-called local sources, with distances up to tens of Mpc, for which the emitted UHECR will not have been as diffused as for farther sources and may still maintain some information about the source location (Lang et al. 2021). It is common to consider every source as a standard candle with an effective spectral index but with different cosmic ray luminosities,  $L_{CR}$ . The observed luminosity in  $\gamma$  rays,  $L_\gamma^{\text{obs}}$  has previously been used as a possible proxy (Abdul Halim et al. 2023a, 2024; Partenheimer et al. 2024). However, a bad agreement between model and data is found with this assumption, in particular due to a strong contribution from Mkn 421, an AGN located at  $\sim 130$  Mpc. In this section, we explore the assumption of using  $L_\gamma^{\text{obs}}$  as a proxy for  $L_{CR}$  in AGN and argue that the intrinsic luminosity  $L_\gamma^{\text{int}}$  may be a more robust assumption.

The Hillas (1984) condition is the minimum requirement when considering astrophysical objects as possible accelerators. The lobes, knots, and hotspots of AGN satisfy the Hillas condition for acceleration up to the ultra-high-energy scale (Alves Batista et al. 2019). AGN also satisfy the luminosity condition (Matthews et al. 2018a; Alves Batista et al. 2019), and can explain the different observed UHECR data (Eichmann et al. 2018; Eichmann 2019; Eichmann et al. 2022; de Oliveira & de Souza 2022, 2023).

Several sites in the structure of AGN have been proposed to be suitable for particle acceleration (see Matthews et al. (2020); Rieger (2022) for reviews), for example: the neighborhood of the supermassive black hole (Katsoulakos & Rieger 2018; Coimbra-Araújo & Anjos 2020; Coimbra-Araújo & dos Anjos 2022); parsec- and kiloparsec-scale jet (Rodrigues et al. 2018; Seo et al. 2023, 2024); backflow of the jet material (Matthews et al. 2018a); the termination shock (Cerutti, Benoît & Giacinti, Gwenaél 2023); and the lobes (O’Sullivan et al. 2009).

### 2.1. Gamma rays in jets

The broadband spectral energy distribution (SED) of jetted AGN have been measured from radio to  $\gamma$  rays (Blandford et al. 2019). The SED has a characteristic double-peak shape, whose origin is still under debate. The lower energy peak is normally attributed to synchrotron radiation from leptonic and hadronic CRs accelerated down the jet (Dermer & Menon 2009). As for the higher-energy peak, the most common hypotheses rely on the upscattering of low-energy

photons to  $\gamma$ -ray energies, by very high- and ultra-high-energy CRs, via inverse Compton (IC) processes. In a lepton-dominated scenario, high-energy electrons and positrons will emit synchrotron radiation while being accelerated in the jet, and upscatter low-frequency (radio through X-rays) synchrotron photons up to  $\gamma$ -ray energies (Finke et al. 2008). This process is known as synchrotron self-Compton (SSC) since the synchrotron photons are emitted in the same region as the  $\gamma$  ray photons. Thermal photons from the broad and narrow line regions, the accretion disk, and the torus can also be upscattered via IC processes, contributing to the  $\gamma$ -ray emission. These emission models are known as external Compton (EC) models (Böttcher et al. 2013).

The detection of X-ray and  $\gamma$  rays demonstrated the existence of regions of particle acceleration along AGN's jets (Blandford et al. 2019). The acceleration of hadrons also must occur at least as efficiently as electrons (Atoyan & Dermer 2004). Hadronic contributions are then added to the leptonic emission in the form of proton synchrotron radiation and through pion decays. For proton-proton reactions with energies of  $\sim 1$  EeV could be responsible for the production of  $\gamma$  rays, via neutral pion decay, with energies  $\epsilon_\gamma \sim 0.1$  EeV. Due to the increased number of intermediate reactions,  $\gamma$  rays originating from charged pion decays require even higher proton energies. Proton-photon interactions can also be responsible for  $\gamma$  ray creation through photomeson or photopair production (Boettcher et al. 2012). In general,  $\gamma$  rays from pions' decay carry approximately 10% of the energy of one UHE proton. Then, assuming that the TeV  $\gamma$  ray has a hadronic origin will imply the existence of UHECR in the PeV scale. However, it is important to note that extragalactic  $\gamma$  rays with energies  $\sim$  EeV are not expected to reach Earth, because of the strong absorption by extragalactic background light (EBL) (Saldana-Lopez et al. 2021).

The most common geometry of jet emission models consists in the particles being accelerated in a compact region propagating at relativistic speeds down the jet. In this region, also known as the *blob*, particles move with a bulk Lorentz factor  $\Gamma_b$  along the jet axis while emitting photons isotropically in the *blob*'s rest frame. For highly relativistic motions ( $\Gamma_b \gg 1$ ), an isotropic emission in the *blob*'s co-moving frame will be observed on Earth as a beamed emission, with a beaming angle  $\theta_{\text{beam}} = \Gamma_b^{-1}$  (Dermer & Menon 2009).

Relativistic transformations of the photon energy and emission angle will impact the observed photon flux. The intrinsic and observed energy of a photon,  $\epsilon_\gamma^{\text{int}}$  and  $\epsilon_\gamma^{\text{obs}}$  respectively, are related by the Doppler factor  $\mathcal{D}$  defined as

$$\mathcal{D} \equiv \frac{\epsilon_\gamma^{\text{obs}}}{\epsilon_\gamma^{\text{int}}} = \frac{1}{\Gamma_b (1 - \beta_b \cos \theta)}, \quad (1)$$

where  $\beta_b$  is the normalized velocity of the *blob*, and  $\theta$  is the angle between the jet axis and Earth's line of sight.

The ratio between the observed flux density  $F_\gamma^{\text{obs}}$  of photons on Earth and the intrinsic photon flux density  $F_\gamma^{\text{int}}$  is

$$\frac{F_\gamma^{\text{obs}}}{F_\gamma^{\text{int}}} = \frac{\nu_\gamma^{\text{obs}}}{\nu_\gamma^{\text{int}}} \frac{d\nu_\gamma^{\text{int}}}{d\nu_\gamma^{\text{obs}}} \frac{dN_\gamma^{\text{obs}}}{dN_\gamma^{\text{int}}} \frac{dt_\gamma^{\text{int}}}{dt_\gamma^{\text{obs}}} \frac{d\Omega_\gamma^{\text{int}}}{d\Omega_\gamma^{\text{obs}}}, \quad (2)$$

where  $d\Omega = dA/d_L^2$ , and  $d_L^2$  is the invariant luminosity distance. From eq. (2), it is possible to show that the observed flux of photons at Earth,  $\Phi_\gamma^{\text{obs}}$ , and therefore the observed luminosity  $L_\gamma^{\text{obs}}$ , is boosted by a factor  $\mathcal{D}^4$  in relation to the intrinsic luminosity  $L_\gamma^{\text{int}}$  (Boettcher et al. 2012),  $L_\gamma^{\text{obs}} = \mathcal{D}^4 L_\gamma^{\text{int}}$ .

## 2.2. UHECR acceleration in AGNs

UHECRs should be accelerated along the jet by different mechanisms in different regions (Matthews et al. 2020; Rieger 2022; Seo et al. 2023, 2024). Magnetic reconnection can be present at the highly magnetized jet base (Medina-Torrejón et al. 2021). Diffusive shock acceleration should dominate in the shocked regions of the jet beam, backflow, and termination shock. Shear acceleration will occur in regions of high velocity gradients, caused by the highly relativistic jet, and even in the neighborhood of the termination shock (Cerutti, Benoit & Giacinti, Gwenael 2023). Acceleration by Fermi II is possible in turbulent regions of the lobes. Only UHECR accelerated in the relativistic beamed plasma is subject to the beamed effect.

One possibility is the acceleration in blobs inside the jet beam (Rodrigues et al. 2018; Zhang & Murase 2023). The cosmic ray emission must be isotropic in the blob rest frame, so relativistic beaming is expected in the lab rest frame. In general, highly relativistic shocks are not efficient UHECR accelerators, and mildly relativistic shocks are more promising (Lemoine & Pelletier 2010; Reville & Bell 2014; Bell et al. 2017; Matthews et al. 2018a). Even the latter can present large flux corrections due to Doppler factors, since the observed luminosity depends on  $\mathcal{D}^4 = \left(\frac{1+\beta}{1-\beta}\right)^2 \sim 3 - 80$ , for  $\beta \sim 0.5 - 0.8$  and line of sight jets. However, the angular distribution of UHECR is likely to be isotropized (in

the lab frame) still in the source region since these particles will still cross the magnetized jet and the lobes before escaping, both with complex magnetic field structure, being the jet itself subject to turbulences and the presence of knots (Goodger et al. 2009; Dubey et al. 2023; Mattia, G. et al. 2023).

Consider the propagation and possible acceleration of UHECR along the kpc-scale jet. Combining hydrodynamics and Monte Carlo simulations, Seo et al. (2023, 2024) found that the main mechanism accelerating UHECR above a few EeV is the relativistic shear acceleration at the interface jet-backflow. Combining magnetohydrodynamics with Particle-in-Cell simulations, Mbarek & Caprioli (2019) made a detailed study of the angular distribution for the UHECR emission on the kpc-scale jet. The angular distribution of UHECR accelerated depends mainly on the toroidal component of the jet magnetic field, able to disperse (isotropic emission) or collimate (anisotropic emission) particles. However, the emission direction is also determined by the deflections inside the cocoon. In the anisotropic scenario, only about half of the particles were collimated, and inside an angle larger than  $\Gamma_{jet}^{-1}$ .

As AGN's jet inflates lobes (Morganti 2017; Hardcastle & Krause 2014; Turner et al. 2022) the UHECR beam should cross them before reaching the extragalactic medium. Due to its extension and presence of turbulent/filamentary magnetic field (Carilli & Barthel 1996; Massaro & Ajello 2011; Hardcastle & Krause 2014; Andati et al. 2024; Guidetti et al. 2011; Sun, Xiao-na et al. 2016; Wykes et al. 2014, 2015), the UHECR scatter inside the lobes, losing its directional information. The scattering length of a UHECR can be approximated as (O'Sullivan et al. 2009; Lang et al. 2020)

$$\lambda_{scatt} \sim \kappa^2 \ell_c \left( \frac{r_L}{\ell_c} \right)^\delta, \quad (3)$$

where  $\kappa^2 = B_0^2/\delta B^2$ ,  $\ell_c$  is the coherence length of the magnetic field,  $\delta$  is the diffusion coefficient, and

$$r_L \approx \frac{E/\text{EeV}}{Z} \frac{1 \text{ kpc}}{B_0/\mu\text{G}}, \quad (4)$$

is the gyroradius of the UHECR of charge  $Z$ .  $B_0$  is the large-scale and  $\delta B$  is the turbulent components of the magnetic field.

The lobes extend across  $R \sim 100$  kpc with magnetic fields  $\sim 1 - 10 \mu\text{G}$  (Massaro & Ajello 2011; Sun, Xiao-na et al. 2016; Wykes et al. 2015; Hardcastle et al. 2015; Andati et al. 2024). The coherence length of the magnetic field is assumed  $\ell_c \sim 0.1R \sim 10$  kpc (Adebahr, B. et al. 2019; O'Sullivan et al. 2009). If  $\lambda_{scatt}$  is smaller than  $R$ , the UHECR will suffer at least one scattering inside the lobes, losing its directional information. The major energy dissipation of the jet occurs in  $\sim \text{pc}$  scale from the jet base (Harvey et al. 2020; Shukla & Mannheim 2020), then considering  $\lambda_{scatt} \sim R$ , we get the energy threshold for one scattering

$$E_{scatt} \sim (Z \times 10 \text{ EeV}) \ell_{10} B_{\mu\text{G}} \left( \frac{10R_{100}}{\ell_{10}\kappa^2} \right)^{1/\delta}, \quad (5)$$

where  $\ell_{10} = \ell/10$  kpc,  $R_{100} = R/100$  kpc, and  $B_{\mu\text{G}} = B_0/\mu\text{G}$ . In a conservative estimation, we can take  $\kappa \approx 1$  ( $B_0 \sim \delta B$ ), and  $\delta = 2$ ,

$$E_{scatt} \sim (Z \times 30 \text{ EeV}) \delta B_{\mu\text{G}} \sqrt{\ell_{10} R_{100}}. \quad (6)$$

Even if accelerated in relativistic blobs inside the jet, protons with energies up to  $\sim 30$  EeV will lose their directional information in the source, being isotropized while traveling through the lobes. Based on source limitations (like Hillas' energy) and results of the Pierre Auger Collaboration (Mayotte et al. 2023) a mixed composition is expected. The data from the Pierre Auger Collaboration indicates  $\langle Z \rangle \sim 1.7 - 5$  at 10 EeV, with  $\langle Z \rangle$  increasing with energy (Aab et al. 2018b; Abdul Halim et al. 2023b; Mayotte et al. 2023). The proton fraction becomes negligible above 10 EeV (Mayotte et al. 2023). Taking  $Z \sim 5$  we get  $E_{scatt} \sim 150$  EeV, encompassing all the detected UHECR. This value can still be large since the photodisintegration makes the composition lighter after the propagation from the source.

This estimation depends on the position of the accelerator on the jet. The scattering can be inefficient if the acceleration occurs mainly on the termination shocks, observed as the hotspot found in FR II radio galaxies (Hardcastle et al. 2007; Snios et al. 2020). As relativistic shocks, the termination shocks are poor accelerators of UHECR (Araudo et al. 2017). Still, in a recent work, Cerutti, Benoît & Giacinti, Gwenael (2023) found that particles can be efficiently accelerated up to  $\sim 10^{20}$  eV by crossing a cavity behind the termination shock. In this case it is unclear if a possible beamed emission will be sustained after leaving the acceleration region. The magnetic field of the vortex downstream of the cavity or of the hotspot itself might decollimate the beam, at least partially.

### 2.3. $\gamma$ -ray luminosity as proxy for UHECR luminosity

If particle acceleration occurs in the jet of AGNs, it is reasonable to assume that a fraction of the jet kinetic power will be converted into UHECR kinetic energy (Eichmann et al. 2018; Eichmann 2019; Matthews & Taylor 2021). The intrinsic  $\gamma$ -ray luminosity is significantly correlated with the jet power of AGN from different categories (Nemmen et al. 2012; Chen et al. 2023). In addition,  $\gamma$ -ray emission is linked to particle acceleration and interactions in its neighborhoods (Reville & Bell 2014; Zhang & Murase 2023, e.g.). In this way, using  $\gamma$ -ray luminosity as a possible normalization for the UHECR flux from different sources is well justified. Nevertheless, when considering the  $\gamma$  rays emitted from particles accelerated in relativistic blobs moving along the jet, the  $\gamma$ -ray flux suffers a Doppler boost in the jet direction, while the same is unlikely for UHECR emission.

Assuming that the UHECR emission scales with the jet power and it is not beamed, the use of  $L_\gamma^{obs}$  as a proxy for  $L_{CR}$  overestimates the UHECR luminosity by a factor  $\sim \mathcal{D}^4$ . This fact becomes especially important when different classes of AGNs are taken into account in the same analysis, such as radio galaxies and blazars. Due to the viewing angle, radio galaxies (RG) have a mean Doppler factor  $\mathcal{D}_{RG} \sim 2.6$  (Ye et al. 2023), while for BL Lacs (BLL),  $\mathcal{D}_{BLL} \sim 10$  (Zhang et al. 2020; Ye et al. 2023). Since the observed luminosity is proportional to  $\mathcal{D}^4$ , this overestimates the UHECR flux from BLL when compared to RG on average by a factor of  $\frac{\mathcal{D}_{BLL}^4}{\mathcal{D}_{RG}^4} \sim 200$ . To remove this bias, it is necessary to consider the cosmic ray luminosity ( $L_{CR}$ ) as being proportional to the intrinsic  $\gamma$ -ray luminosity  $L_\gamma^{int}$  instead, where  $L_\gamma^{int} = \mathcal{D}^{-4} L_\gamma^{obs}$ .

## 3. IMPLICATIONS FOR THE SEARCH FOR SOURCES

In this section, we explore the implications of using the observed and intrinsic  $\gamma$ -ray luminosity of sources as proxy for the UHECR luminosity. We will use the  $\gamma$ AGN catalog selected from the analysis of the Pierre Auger Collaboration (Abdul Halim et al. 2024). The selection contains jetted AGNs measured with the Fermi-LAT with a  $\gamma$ -ray flux  $> 3.3 \times 10^{-11} \text{ cm}^{-2} \text{ s}^{-1}$  between 10 GeV and 1 TeV on the 3FHL catalog of Fermi (Ajello et al. 2017). The  $\mathcal{D}$  values are taken from different references (see Table 1). Due to the range of values found for some sources, two sets of proxies were created,  $L_\gamma^{int, \min} = \mathcal{D}_{\max}^{-4} L_\gamma^{obs}$  and  $L_\gamma^{int, \max} = \mathcal{D}_{\min}^{-4} L_\gamma^{obs}$ . The  $\mathcal{D}$  values were not found for all BLL in the analysis. In these cases, conservative ( $\mathcal{D} = 1$ ) and expected ( $\mathcal{D} = 10$ ) values were employed.

Figure 1 shows the different luminosity weights used as proxies for the UHECR luminosity. The circle size represents the expected flux on Earth and is linearly proportional to the luminosity of each source. Sources with  $L_\gamma$  smaller than 1% of the largest value in each panel are shown as black diamonds of fixed size. When comparing panels (a) with (b) and (c), it is clear the importance of considering the Doppler factor on the contribution of each source. Even though Mkn 421 is the dominant source using  $L_\gamma^{obs}$  (case a), it becomes negligible in any scenario where Doppler boosting effects are corrected (cases b and c). The radio galaxies Cen A and Fornax A are the most significant sources in case (b). Cen A, PMN J0816-1311, and PKS 0521-36 dominate case (c). In both cases, the contribution from two distant sources ( $> 200$  Mpc) that are not in the field of view of the Pierre Auger Observatory, Mkn 180 and SBS 1646+499, is also remarkable.

### 3.1. Results from the combined fit

The proxies for the luminosity,  $L_{CR}$ , only provide an estimation of the emissivities of each source considered. UHECR undergo different energy and primary-dependent energy losses during propagation, which modulate the final spectrum and composition. For that reason, the final contribution from each source will strongly rely on the astrophysical model assumed for the sources, i.e., their injected spectra and compositions. To take this into effect, we have performed a combined spectrum and composition fit, following the approach of previous works by the Pierre Auger Collaboration (Aab et al. 2017; Abdul Halim et al. 2024). 1-D simulations in CRPropa3 (Batista et al. 2016) were performed in a uniform grid of energy (from  $10^{18}$  eV to  $10^{22}$  eV with 10 bins per decade), and distance (from 3 to 3342 Mpc in 118 bins in log) for each of the five representative primaries,  $^1\text{H}$ ,  $^4\text{He}$ ,  $^{14}\text{N}$ ,  $^{28}\text{Si}$ , and  $^{56}\text{Fe}$ . All the energy losses were considered and the EBL model of Gilmore et al. (2012) was considered. A smearing was introduced in the arrival directions via a Von Mises-Fisher distribution (Fisher 1953) similar to that of Abdul Halim et al. (2024), with  $\Delta_0 = 5^\circ$  and  $R_0 = 10$  EV. The direction-dependent exposure of the experiment was taken into account to consider only events with zenith angles smaller than 60 degrees. The effective spectrum of each source was fitted to

$$dN/dE(E) = \begin{cases} N_s F_i E^{-\Gamma}, & \text{for } E \leq Z_i R_{\max} \\ N_s F_i E^{-\Gamma} e^{(1-E/(Z_i R_{\max}))}, & \text{for } E > Z_i R_{\max} \end{cases}, \quad (7)$$

where the free parameters of the fit are the spectral index,  $\Gamma$ , the maximum rigidity at the sources,  $R_{\max}$ , the normalizations,  $N_s$ , and the contribution of each species,  $F_i$ .  $F_i$  is defined as the total contribution of a primary between 1 EeV and the corresponding maximum energy,  $ZR_{\max}$ . This definition relates to that of Aab et al. (2017),  $f_i$  (i.e., the relative contribution of each primary for an energy bin below the maximum energy of protons) as  $f_i = F_i / (Z_i R_{\max})^{(\Gamma-1)}$ . Such quantity was chosen because it provides a more robust minimization procedure for the fit. The sources were divided into two classes: a homogeneous distribution of background sources with equal emissivity and the so-called local sources, whose individual emissivities are modulated by the values in Table 1. The relative contribution of local and background sources is given by the fit parameter  $\alpha = J_{\text{local}}(E = 10^{19.5} \text{ eV}) / J_{\text{background}}(E = 10^{19.5} \text{ eV})$ .

The simulations are convolved with the weights described above and compared to the spectral data above  $10^{18.7} \text{ eV}$  from Verzi (2020) and measurements of the first and second moments of the  $X_{\max}$  distributions from Yushkov (2020)<sup>1</sup>. We use a deviance function, which maps a Poissonian likelihood function into a  $\chi^2$ -like distribution by comparing it to the saturated likelihood. The two upper limits on the spectrum are incorporated into the likelihood function to avoid an overcontribution of local sources. The arrival directions distribution and full  $X_{\max}$  distributions (instead of its moments) could not be used due to the non-availability of these data to the community outside of the Pierre Auger collaboration.

The systematic uncertainties in the spectrum and  $X_{\max}$  were addressed by performing a new fit with the data shifted by  $\pm 14\%$  for the energy and  $\pm 1\sigma$  for the  $X_{\max}(E)$  according to Aab et al. (2014). Resulting in a total of 9 fits for each of the cases (a), (b), and (c). The fit achieved its best description with  $E \rightarrow E + 14\%$  and no shift in  $X_{\max}$ .

Figure 2 shows the spectrum and  $X_{\max}$  moments for the best fit of the  $L_{\gamma}^{\text{int},\text{min}}$  scenario (case b). Due to the contribution of local sources being significant only at the highest energies, where statistics are poorer, the spectral index, maximum rigidity, and primary fractions change very little between the best fits for each of the cases. Similarly to the previous results found by the Pierre Auger Collaboration, a very hard spectrum with  $\Gamma < 0$  with a strict rigidity cutoff is preferred. Nevertheless, a significant difference can be found in the fraction of the contribution of local sources and total deviance:  $\alpha_{L_{\gamma}^{\text{obs}}} = 0.65\%$ ,  $\alpha_{L_{\gamma}^{\text{int},\text{min}}} = 18.03\%$ , and  $\alpha_{L_{\gamma}^{\text{int},\text{max}}} = 3.81\%$  and  $D_{L_{\gamma}^{\text{int},\text{min}}} - D_{L_{\gamma}^{\text{obs}}} = -12.66$ ,  $D_{L_{\gamma}^{\text{int},\text{max}}} - D_{L_{\gamma}^{\text{obs}}} = -9.73$ , respectively. The data are better fitted with the intrinsic luminosities, and the fit allowed for a higher contribution from the local sources. The reason can be seen in figure 3. A larger contribution from a very local source such as Cen A will result in a total spectrum with a spectral index very similar to the intrinsic spectral index assumed for the sources. When larger relative contributions from farther sources are predicted, an effective spectral index is seen in the combined local source flux. This is mostly due to two effects: the suppression will occur at different energies for sources at different distances, and more UHECR from farther sources will go through photodisintegration, resulting in a larger contribution to lower energies in the spectrum. In conclusion, even before comparing the results of the distribution of arrival directions, the assumptions here proposed improve the description of the data by  $3.12 - 3.56\sigma$ .

Yet, as expected, the most important effect is seen in the distributions of arrival directions. Figure 4 shows the arrival direction maps for  $E > 32 \text{ EeV}$ , as well as the dipole direction  $E > 8 \text{ EeV}$  and  $E > 32 \text{ EeV}$ . The hotspots change for each scenario considered. The dominance of Mkn 421 seen in  $L_{\gamma}^{\text{obs}}$  (case a) vanishes when the new proxies are used, with a dominance of Cen A, Fornax A and Mkn 180 rising for  $L_{\gamma}^{\text{int},\text{min}}$  (case b) and of PMN J0816-1311, Cen A and Mkn 180 for  $L_{\gamma}^{\text{int},\text{max}}$  (case c). For  $L_{\gamma}^{\text{int},\text{min}}$  (case b), the arrival directions are dominated by three main hotspots that are in relative agreement with the two hotspots reported by the Pierre Auger Observatory (Abdul Halim et al. 2023a) and the hotspot reported by the Telescope Array Observatory (Kim et al. 2023).

The agreement of the predicted direction of the dipole with that measured by the Pierre Auger Observatory greatly improves, going from  $10.3 (5.4)\sigma$  away from the measurement for  $> 8(32) \text{ EeV}$  using  $L_{\gamma}^{\text{obs}}$  to  $12.8 (1.5)\sigma$  and  $2.2 (3.0)\sigma$  using  $L_{\gamma}^{\text{int},\text{min}}$  (case b) and  $L_{\gamma}^{\text{int},\text{max}}$  (case c), respectively.

#### 4. SUMMARY AND DISCUSSION

AGN are among the main candidates to accelerate cosmic rays up to  $10^{20} \text{ eV}$ . Different views on the relative contribution from each source have been explored in previous works, leading to a significant change in the agreement with data. In this work, we conciliate these studies with a deep verification of the  $\gamma$ -ray luminosity proxy for UHECR.

- **The association between  $\gamma$  rays and UHECR is weak, but not impossible:**  $\gamma$  rays can have an origin in leptonic or hadronic scenarios. In the hadronic case, the cosmic ray energy necessary to produce a  $\sim \text{TeV}$   $\gamma$

<sup>1</sup> Taken from Pierre Auger's public dataset: <https://www.auger.org/science/public-data/data>

ray is  $\sim$ PeV, considerably below the UHECR regime.  $\gamma$  rays emitted by EeV UHECR will likely have energies not accessible by  $\gamma$ -ray observatories due to EBL attenuation. In this way, the correlation between  $\gamma$  rays and UHECR can be considered weak, although it should not be ignored, since the detection of  $\gamma$  radiation implies the existence of regions where the acceleration of charged particles occurs. Furthermore, the  $\gamma$ -ray luminosity is related to the jet power in AGN, which can be related to its UHECR luminosity;

- **The use of the observed flux of  $\gamma$  rays as proxies for UHECR implicitly assume that both are beamed:** When the  $\gamma$ -ray flux is used as a proxy for the UHECR flux, there is an **implicit hypothesis** that UHECR are subject to the same beaming effect of  $\gamma$  rays. It is unclear if UHECR are accelerated in relativistic blobs as is assumed for  $\gamma$  rays. However, even in that case, the magnetic fields in the acceleration regions, jets and lobes, will likely decollimate the UHECR beam, as shown in numerical studies. This way, the expected emission cone of UHECR is larger than that of  $\gamma$  rays;
- **The correction of the observed flux of  $\gamma$  rays as proxies for UHECR is source dependent and on average decreases the contribution for farther sources:** Assuming that UHECR are not beamed as  $\gamma$  rays, the intrinsic  $\gamma$ -ray luminosity is a better proxy than the observed  $\gamma$ -ray luminosity. The relation between the intrinsic and the observed  $\gamma$ -ray luminosities is given by  $L_\gamma^{\text{int}} = \mathcal{D}^{-4} L_\gamma^{\text{obs}}$ . It becomes more significant when different AGN classes are considered, such as blazars ( $\mathcal{D} \sim 10$ ) and radio galaxies ( $\mathcal{D} \sim 2$ );
- **Using intrinsic  $\gamma$ -ray luminosity as UHECR proxy gives a better fit to the Pierre Auger Observatory data:** A combined fit of spectrum and composition data performs better when  $L_\gamma^{\text{int}}$  is considered. The spectral shape of local sources is changed due to an increase in the relative contribution of closer sources. For the simple combined fit proposed in this work, an improvement of  $3.12 - 3.56\sigma$  is found.
- **Using intrinsic  $\gamma$ -ray luminosity as UHECR proxy conciliates the arrival directions data:** The relative contribution of each source, particularly at the highest energies, is changed for different proxy assumptions. When  $L_\gamma^{\text{int}}$  is considered, the strong expected contribution from Mkn 421 vanishes. The predicted dipole shifts from  $10.3 (5.4)\sigma$  up to  $2.2 (1.5)\sigma$  away from the one measured by the Pierre Auger Observatory. The predicted hotspots also change significantly. In particular, for the  $L_\gamma^{\text{int, min}}$  case, three main hotspots appear in locations similar to two the hotspots measured by the Pierre Auger Observatory and the hotspot measured by the Telescope Array Experiment.

The intrinsic  $\gamma$ -ray luminosity used here appears to be a better proxy than the observed  $\gamma$ -ray luminosity. Since the intrinsic  $\gamma$ -ray luminosity is related to the jet power, it agrees with authors who argue that the UHECR luminosity must scale with the jet power (Eichmann et al. 2018; Matthews & Taylor 2021). In particular, Matthews & Taylor (2021) suggests that radio luminosity is a better proxy for  $L_{\text{CR}}$ , with reservations due to UHECR transport and particular characteristics of different sources.

Our results resonate with other works that get a good description of the UHECR data using AGN catalogs. Using the jet power as a proxy for  $L_{\text{CR}}$ , Eichmann et al. (2018); Eichmann (2019); Eichmann et al. (2022) have obtained a good description of experimental data. The contribution of the radio galaxies Cen A and Fornax A have been proposed as responsible for the dipole and hotspots measured by the Pierre Auger Observatory (Matthews et al. 2018b; de Oliveira & de Souza 2022). Moreover, in contrast to a fully isotropic emission, Rachen & Eichmann (2019) propose that blazars could have an additional beamed UHECR emission. In this work, we neglect that based on the decollimation effect on the source region. Due to the energy dependence on the magnetic scattering of charged particles, the decollimation of a possible UHECR beam will also be energy-dependent. We do not account for this effect here, and it will be addressed in future works.

After leaving the source, the extragalactic and galactic magnetic fields also should decollimate an eventual residual UHECR beam. In this work, we follow the simplistic assumption of blurring the arrival directions due to a turbulent component of the extragalactic magnetic field. The regular component of the EGMF can cause amplification/suppression of sources and a shift of arrival directions, which can be significant even to nearby sources (Lang et al. 2021; de Oliveira & de Souza 2022, 2023) and must be taken into account in a detailed study. However, the EGMF structure seems to have a minor effect in the dipole direction for  $E > 32$  EeV if the flux is dominated by nearby radio galaxies (de Oliveira & de Souza 2023). Deflections by the galactic magnetic field were not taken into account either. A detailed exploration of the effect of the cosmic magnetic fields is beyond the scope of this study, since the

extragalactic and galactic magnetic fields are complex and the effects on UHECRs are still open questions (Bakalová et al. 2023; Harari et al. 2002; Hackstein et al. 2018; de Oliveira & de Souza 2022).

The combined fit used in this work is a simplified version that does not take into account the full  $X_{\max}$  distributions and the arrival direction distribution due to the non-availability of the data. Still, the results shown here for arrival direction maps and dipole indicate that a full fit with the proxies here proposed will increase even further the agreement with the data.

Therefore, even with the intrinsic limitations addressed above, the results of this work strengthen the hypothesis of AGN as candidates for the origin of UHECR and provide the community with a more robust hypothesis about the proxies for  $L_{\text{CR}}$  using  $L_{\gamma}$ . In addition, it potentially conciliate the results using different proxies, since both the radio and the intrinsic  $\gamma$ -ray luminosity scales with the jet power. These assumptions could be used in future studies that aim to model the data or look for correlations in the arrival directions data from the Pierre Auger Observatory and the Telescope Array Experiment.

#### ACKNOWLEDGMENTS

The idea for this work was developed during a series of two joint FAPESP/BAYLAT workshops titled “Astroparticle physics in the era of CTA and SWGO” at the Friedrich-Alexander-Universität Erlangen-Nürnberg and the Instituto de Física de São Carlos, Universidade de São Paulo in 2023 and 2024. We acknowledge the generous support for these workshops by FAPESP (through grant number 2022/01271-7) and BAYLAT. The authors thank Vitor de Souza, James Matthews, and Teresa Bister for reading the paper and making useful comments. CO acknowledges FAPESP Projects 2019/10151-2, 2020/15453-4, and 2021/01089-1. CO acknowledges the National Laboratory for Scientific Computing (LNCC/MCTI, Brazil) for providing HPC resources for the SDumont supercomputer (<http://sdumont.lncc.br>).

#### REFERENCES

- Aab, A., et al. 2014, *Phys. Rev. D*, 90, 122005, doi: [10.1103/PhysRevD.90.122005](https://doi.org/10.1103/PhysRevD.90.122005)
- Aab, A., Abreu, P., Aglietta, M., et al. 2017, *Journal of Cosmology and Astroparticle Physics*, 2017, 038, doi: [10.1088/1475-7516/2017/04/038](https://doi.org/10.1088/1475-7516/2017/04/038)
- . 2018a, *The Astrophysical Journal Letters*, 853, L29, doi: [10.3847/2041-8213/aaa66d](https://doi.org/10.3847/2041-8213/aaa66d)
- . 2018b, *The Astrophysical Journal*, 868, 4, doi: [10.3847/1538-4357/aae689](https://doi.org/10.3847/1538-4357/aae689)
- Abdo, A. A., Ackermann, M., Ajello, M., et al. 2011a, *The Astrophysical Journal*, 736, 131, doi: [10.1088/0004-637X/736/2/131](https://doi.org/10.1088/0004-637X/736/2/131)
- . 2011b, *The Astrophysical Journal*, 727, 129, doi: [10.1088/0004-637X/727/2/129](https://doi.org/10.1088/0004-637X/727/2/129)
- Abdul Halim, A., et al. 2023a, *PoS, ICRC2023*, 252, doi: [10.22323/1.444.0252](https://doi.org/10.22323/1.444.0252)
- Abdul Halim, A., Abreu, P., Aglietta, M., et al. 2023b, in *Proceedings of 38th International Cosmic Ray Conference — PoS(ICRC2023)*, Vol. 444, 438, doi: [10.22323/1.444.0438](https://doi.org/10.22323/1.444.0438)
- Abdul Halim, A., Abreu, P., Aglietta, M., et al. 2024, *Journal of Cosmology and Astroparticle Physics*, 2024, 022, doi: [10.1088/1475-7516/2024/01/022](https://doi.org/10.1088/1475-7516/2024/01/022)
- Abreu, P., Aglietta, M., Albury, J. M., et al. 2022, *The Astrophysical Journal*, 935, 170, doi: [10.3847/1538-4357/ac7d4e](https://doi.org/10.3847/1538-4357/ac7d4e)
- Abu-Zayyad, T., Aida, R., Allen, M., et al. 2012, *Nuclear Instruments and Methods in Physics Research Section A: Accelerators, Spectrometers, Detectors and Associated Equipment*, 689, 87, doi: <https://doi.org/10.1016/j.nima.2012.05.079>
- Acciari, M. V. A., Ansoldi, S., Antonelli, L. A., et al. 2020a, *Monthly Notices of the Royal Astronomical Society*, 496, 3912, doi: [10.1093/mnras/staa1702](https://doi.org/10.1093/mnras/staa1702)
- Acciari, V. A., Ansoldi, S., Antonelli, L. A., et al. 2020b, *The Astrophysical Journal Supplement Series*, 247, 16, doi: [10.3847/1538-4365/ab5b98](https://doi.org/10.3847/1538-4365/ab5b98)
- Adebahr, B., Brienza, M., & Morganti, R. 2019, *A&A*, 622, A209, doi: [10.1051/0004-6361/201833988](https://doi.org/10.1051/0004-6361/201833988)
- Ahnen, M. L., Ansoldi, S., Antonelli, L. A., et al. 2017, *A&A*, 603, A25, doi: [10.1051/0004-6361/201630347](https://doi.org/10.1051/0004-6361/201630347)
- Ajello, M., Atwood, W. B., Baldini, L., et al. 2017, *The Astrophysical Journal Supplement Series*, 232, 18, doi: [10.3847/1538-4365/aa8221](https://doi.org/10.3847/1538-4365/aa8221)
- Aleksić, J., Ansoldi, S., Antonelli, L. A., et al. 2014, *A&A*, 564, A5, doi: [10.1051/0004-6361/201322951](https://doi.org/10.1051/0004-6361/201322951)
- Aloisio, R., Boncioli, D., di Matteo, A., et al. 2017, *Journal of Cosmology and Astroparticle Physics*, 2017, 009, doi: [10.1088/1475-7516/2017/11/009](https://doi.org/10.1088/1475-7516/2017/11/009)
- Alves Batista, R., Biteau, J., Bustamante, M., et al. 2019, *Frontiers in Astronomy and Space Sciences*, 6, doi: [10.3389/fspas.2019.00023](https://doi.org/10.3389/fspas.2019.00023)



- Andati, L. A. L., Baidoo, L. M., Ramaila, A. J. T., et al. 2024, *Monthly Notices of the Royal Astronomical Society*, 529, 1626, doi: [10.1093/mnras/stae598](https://doi.org/10.1093/mnras/stae598)
- Araudo, A. T., Bell, A. R., Blundell, K. M., & Matthews, J. H. 2017, *Monthly Notices of the Royal Astronomical Society*, 473, 3500, doi: [10.1093/mnras/stx2552](https://doi.org/10.1093/mnras/stx2552)
- Atoyan, A., & Dermer, C. 2004, *New Astronomy Reviews*, 48, 381, doi: <https://doi.org/10.1016/j.newar.2003.12.046>
- Bakalová, A., Vícha, J., & Trávníček, P. 2023, *Journal of Cosmology and Astroparticle Physics*, 2023, 016, doi: [10.1088/1475-7516/2023/12/016](https://doi.org/10.1088/1475-7516/2023/12/016)
- Batista, R. A., Dundovic, A., Erdmann, M., et al. 2016, *Journal of Cosmology and Astroparticle Physics*, 2016, 038, doi: [10.1088/1475-7516/2016/05/038](https://doi.org/10.1088/1475-7516/2016/05/038)
- Bell, A. R., Araudo, A. T., Matthews, J. H., & Blundell, K. M. 2017, *Monthly Notices of the Royal Astronomical Society*, 473, 2364, doi: [10.1093/mnras/stx2485](https://doi.org/10.1093/mnras/stx2485)
- Blandford, R., Meier, D., & Readhead, A. 2019, *Annual Review of Astronomy and Astrophysics*, 57, 467, doi: <https://doi.org/10.1146/annurev-astro-081817-051948>
- Boettcher, M., Harris, D. E., & Krawczynski, H. 2012, *Relativistic jets from active galactic nuclei* (Wiley-VCH)
- Böttcher, M., Reimer, A., Sweeney, K., & Prakash, A. 2013, *The Astrophysical Journal*, 768, 54, doi: [10.1088/0004-637X/768/1/54](https://doi.org/10.1088/0004-637X/768/1/54)
- Carilli, C., & Barthel, P. 1996, *The astronomy and astrophysics review*, 7, 1. <https://doi.org/10.1007/s001590050001>
- Cerutti, Benoît, & Giacinti, Gwenael. 2023, *A&A*, 676, A23, doi: [10.1051/0004-6361/202346481](https://doi.org/10.1051/0004-6361/202346481)
- Chen, Y., Gu, Q., Fan, J., et al. 2023, *Monthly Notices of the Royal Astronomical Society*, 519, 6199, doi: [10.1093/mnras/stad065](https://doi.org/10.1093/mnras/stad065)
- Coimbra-Araújo, C. H., & Anjos, R. C. 2020, *Classical and Quantum Gravity*, 38, 015007, doi: [10.1088/1361-6382/abc189](https://doi.org/10.1088/1361-6382/abc189)
- Coimbra-Araújo, C. H., & dos Anjos, R. C. 2022, *Galaxies*, 10, doi: [10.3390/galaxies10040084](https://doi.org/10.3390/galaxies10040084)
- de Oliveira, C., & de Souza, V. 2022, *The Astrophysical Journal*, 925, 42, doi: [10.3847/1538-4357/ac3753](https://doi.org/10.3847/1538-4357/ac3753)
- . 2023, *Journal of Cosmology and Astroparticle Physics*, 2023, 058, doi: [10.1088/1475-7516/2023/07/058](https://doi.org/10.1088/1475-7516/2023/07/058)
- Dermer, C. D., & Menon, G. 2009, *High energy radiation from black holes: gamma rays, cosmic rays, and neutrinos* (Princeton Series in Astrophysics)
- di Matteo, A. et al. for the Pierre Auger and Telescope Array collaborations. 2023, *EPJ Web Conf.*, 283, 03002, doi: [10.1051/epjconf/202328303002](https://doi.org/10.1051/epjconf/202328303002)
- Dubey, R. P., Fendt, C., & Vaidya, B. 2023, *The Astrophysical Journal*, 952, 1, doi: [10.3847/1538-4357/ace0bf](https://doi.org/10.3847/1538-4357/ace0bf)
- Eichmann, B. 2019, *Journal of Cosmology and Astroparticle Physics*, 2019, 009, doi: [10.1088/1475-7516/2019/05/009](https://doi.org/10.1088/1475-7516/2019/05/009)
- Eichmann, B., Kachelrieß, M., & Oikonomou, F. 2022, *Journal of Cosmology and Astroparticle Physics*, 2022, 006, doi: [10.1088/1475-7516/2022/07/006](https://doi.org/10.1088/1475-7516/2022/07/006)
- Eichmann, B., Rachen, J., Merten, L., van Vliet, A., & Tjus, J. B. 2018, *Journal of Cosmology and Astroparticle Physics*, 2018, 036, doi: [10.1088/1475-7516/2018/02/036](https://doi.org/10.1088/1475-7516/2018/02/036)
- Finke, J. D., Dermer, C. D., & Böttcher, M. 2008, *The Astrophysical Journal*, 686, 181, doi: [10.1086/590900](https://doi.org/10.1086/590900)
- Fisher, R. 1953, *Proceedings of the Royal Society of London Series A*, 217, 295, doi: [10.1098/rspa.1953.0064](https://doi.org/10.1098/rspa.1953.0064)
- Gilmore, R. C., Somerville, R. S., Primack, J. R., & Domínguez, A. 2012, *Monthly Notices of the Royal Astronomical Society*, 422, 3189, doi: [10.1111/j.1365-2966.2012.20841.x](https://doi.org/10.1111/j.1365-2966.2012.20841.x)
- Goodger, J. L., Hardcastle, M. J., Croston, J. H., et al. 2009, *The Astrophysical Journal*, 708, 675, doi: [10.1088/0004-637X/708/1/675](https://doi.org/10.1088/0004-637X/708/1/675)
- Guidetti, D., Laing, R. A., Bridle, A. H., Parma, P., & Gregorini, L. 2011, *Monthly Notices of the Royal Astronomical Society*, 413, 2525, doi: [10.1111/j.1365-2966.2011.18321.x](https://doi.org/10.1111/j.1365-2966.2011.18321.x)
- Hackstein, S., Vazza, F., Brügggen, M., Sorce, J. G., & Gottlöber, S. 2018, *Monthly Notices of the Royal Astronomical Society*, 475, 2519, doi: [10.1093/mnras/stx3354](https://doi.org/10.1093/mnras/stx3354)
- Harari, D., Mollerach, S., Roulet, E., & Sánchez, F. 2002, *Journal of High Energy Physics*, 2002, 045, doi: [10.1088/1126-6708/2002/03/045](https://doi.org/10.1088/1126-6708/2002/03/045)
- Hardcastle, M. J., Croston, J. H., & Kraft, R. P. 2007, *The Astrophysical Journal*, 669, 893, doi: [10.1086/521696](https://doi.org/10.1086/521696)
- Hardcastle, M. J., & Krause, M. G. H. 2014, *Monthly Notices of the Royal Astronomical Society*, 443, 1482, doi: [10.1093/mnras/stu1229](https://doi.org/10.1093/mnras/stu1229)
- Hardcastle, M. J., Lenc, E., Birkinshaw, M., et al. 2015, *Monthly Notices of the Royal Astronomical Society*, 455, 3526, doi: [10.1093/mnras/stv2553](https://doi.org/10.1093/mnras/stv2553)
- Harvey, A. L. W., Georganopoulos, M., & Meyer, E. T. 2020, *Nature communications*, 11, 5475
- Hervet, O., Boisson, C., & Sol, H. 2015, *A&A*, 578, A69, doi: [10.1051/0004-6361/201425330](https://doi.org/10.1051/0004-6361/201425330)
- H.E.S.S. Collaboration, Abdalla, H., Abramowski, A., et al. 2018, *A&A*, 619, A71, doi: [10.1051/0004-6361/201832640](https://doi.org/10.1051/0004-6361/201832640)
- HESS Collaboration, Abdalla, H., Abramowski, A., et al. 2018, *Monthly Notices of the Royal Astronomical Society*, 476, 4187, doi: [10.1093/mnras/sty439](https://doi.org/10.1093/mnras/sty439)

- Hillas, A. M. 1984, *Annual Review of Astronomy and Astrophysics*, 22, 425, doi: <https://doi.org/10.1146/annurev.aa.22.090184.002233>
- Katsoulakos, G., & Rieger, F. M. 2018, *The Astrophysical Journal*, 852, 112, doi: [10.3847/1538-4357/aaa003](https://doi.org/10.3847/1538-4357/aaa003)
- Kim, J., Ivanov, D., Kawata, K., Sagawa, H., & Thomson, G. 2023, *PoS, ICRC2023*, 244, doi: [10.22323/1.444.0244](https://doi.org/10.22323/1.444.0244)
- Kotera, K., & Olinto, A. V. 2011, *Annual Review of Astronomy and Astrophysics*, 49, 119
- Lang, R. G., Taylor, A. M., Ahlers, M., & de Souza, V. 2020, *Phys. Rev. D*, 102, 063012, doi: [10.1103/PhysRevD.102.063012](https://doi.org/10.1103/PhysRevD.102.063012)
- Lang, R. G., Taylor, A. M., & de Souza, V. 2021, *Phys. Rev. D*, 103, doi: [10.1103/physrevd.103.063005](https://doi.org/10.1103/physrevd.103.063005)
- Lemoine, M., & Pelletier, G. 2010, *Monthly Notices of the Royal Astronomical Society*, 402, 321, doi: [10.1111/j.1365-2966.2009.15869.x](https://doi.org/10.1111/j.1365-2966.2009.15869.x)
- Linsley, J. 1963, *Phys. Rev. Lett.*, 10, 146, doi: [10.1103/PhysRevLett.10.146](https://doi.org/10.1103/PhysRevLett.10.146)
- Liodakis, I., Hovatta, T., Huppenkothen, D., et al. 2018, *The Astrophysical Journal*, 866, 137, doi: [10.3847/1538-4357/aae2b7](https://doi.org/10.3847/1538-4357/aae2b7)
- Lister, M. L., Homan, D. C., Kovalev, Y. Y., et al. 2020, *The Astrophysical Journal*, 899, 141, doi: [10.3847/1538-4357/aba18d](https://doi.org/10.3847/1538-4357/aba18d)
- MAGIC Collaboration, Acciari, V. A., Ansoldi, S., et al. 2020a, *Monthly Notices of the Royal Astronomical Society*, 492, 5354, doi: [10.1093/mnras/staa014](https://doi.org/10.1093/mnras/staa014)
- MAGIC Collaboration, Acciari, V. A., Ansoldi, S., et al. 2020b, *A&A*, 638, A14, doi: [10.1051/0004-6361/201935450](https://doi.org/10.1051/0004-6361/201935450)
- Massaro, F., & Ajello, M. 2011, *The Astrophysical Journal Letters*, 729, L12, doi: [10.1088/2041-8205/729/1/L12](https://doi.org/10.1088/2041-8205/729/1/L12)
- Matthews, J. H., Bell, A. R., & Blundell, K. M. 2020, *New Astronomy Reviews*, 89, 101543, doi: <https://doi.org/10.1016/j.newar.2020.101543>
- Matthews, J. H., Bell, A. R., Blundell, K. M., & Araudo, A. T. 2018a, *Monthly Notices of the Royal Astronomical Society*, 482, 4303
- . 2018b, *Monthly Notices of the Royal Astronomical Society: Letters*, 479, L76, doi: [10.1093/mnrasl/sly099](https://doi.org/10.1093/mnrasl/sly099)
- Matthews, J. H., & Taylor, A. M. 2021, *Monthly Notices of the Royal Astronomical Society*, 503, 5948, doi: [10.1093/mnras/stab758](https://doi.org/10.1093/mnras/stab758)
- Mattia, G., Del Zanna, L., Bugli, M., et al. 2023, *A&A*, 679, A49, doi: [10.1051/0004-6361/202347126](https://doi.org/10.1051/0004-6361/202347126)
- Mayotte, E. W., Abdul Halim, A., Abreu, P., et al. 2023, in *Proceedings of 38th International Cosmic Ray Conference — PoS(ICRC2023)*, Vol. 444, 365, doi: [10.22323/1.444.0365](https://doi.org/10.22323/1.444.0365)
- Mbarek, R., & Caprioli, D. 2019, *The Astrophysical Journal*, 886, 8, doi: [10.3847/1538-4357/ab4a08](https://doi.org/10.3847/1538-4357/ab4a08)
- Medina-Torrejón, T. E., de Gouveia Dal Pino, E. M., Kadowaki, L. H. S., et al. 2021, *The Astrophysical Journal*, 908, 193, doi: [10.3847/1538-4357/abd6c2](https://doi.org/10.3847/1538-4357/abd6c2)
- Morganti, R. 2017, *Frontiers in Astronomy and Space Sciences*, 4, doi: [10.3389/fspas.2017.00042](https://doi.org/10.3389/fspas.2017.00042)
- Nagano, M., & Watson, A. A. 2000, *Rev. Mod. Phys.*, 72, 689, doi: [10.1103/RevModPhys.72.689](https://doi.org/10.1103/RevModPhys.72.689)
- Nemmen, R. S., Georganopoulos, M., Guiriec, S., et al. 2012, *Science*, 338, 1445, doi: [10.1126/science.1227416](https://doi.org/10.1126/science.1227416)
- O'Sullivan, S., Reville, B., & Taylor, A. M. 2009, *Monthly Notices of the Royal Astronomical Society*, 400, 248, doi: [10.1111/j.1365-2966.2009.15442.x](https://doi.org/10.1111/j.1365-2966.2009.15442.x)
- Partenheimer, A., Fang, K., Batista, R. A., & de Almeida, R. M. 2024, *The Astrophysical Journal Letters*, 967, L15, doi: [10.3847/2041-8213/ad4359](https://doi.org/10.3847/2041-8213/ad4359)
- Rachen, J. P., & Eichmann, B. 2019, A parameterized catalog of radio galaxies as ultra-high energy cosmic ray sources. <https://arxiv.org/abs/1909.00261>
- Reville, B., & Bell, A. R. 2014, *Monthly Notices of the Royal Astronomical Society*, 439, 2050, doi: [10.1093/mnras/stu088](https://doi.org/10.1093/mnras/stu088)
- Rieger, F. M. 2022, *Universe*, 8, doi: [10.3390/universe8110607](https://doi.org/10.3390/universe8110607)
- Rodrigues, X., Fedynitch, A., Gao, S., Boncioli, D., & Winter, W. 2018, *The Astrophysical Journal*, 854, 54, doi: [10.3847/1538-4357/aaa7ee](https://doi.org/10.3847/1538-4357/aaa7ee)
- Saldana-Lopez, A., Domínguez, A., Pérez-González, P. G., et al. 2021, *Monthly Notices of the Royal Astronomical Society*, 507, 5144, doi: [10.1093/mnras/stab2393](https://doi.org/10.1093/mnras/stab2393)
- Seo, J., Ryu, D., & Kang, H. 2023, *The Astrophysical Journal*, 944, 199, doi: [10.3847/1538-4357/acb3ba](https://doi.org/10.3847/1538-4357/acb3ba)
- . 2024, *The Astrophysical Journal*, 962, 46, doi: [10.3847/1538-4357/ad182c](https://doi.org/10.3847/1538-4357/ad182c)
- Shukla, A., & Mannheim, K. 2020, *Nature Communications*, 11, 4176
- Snios, B., Johnson, A. C., Nulsen, P. E. J., et al. 2020, *The Astrophysical Journal*, 891, 173, doi: [10.3847/1538-4357/ab737d](https://doi.org/10.3847/1538-4357/ab737d)
- Sun, Xiao-na, Yang, Rui-zhi, Mckinley, Benjamin, & Aharonian, Felix. 2016, *A&A*, 595, A29, doi: [10.1051/0004-6361/201629069](https://doi.org/10.1051/0004-6361/201629069)
- The Pierre Auger Collaboration. 2015, *Nuclear Instruments and Methods in Physics Research Section A: Accelerators, Spectrometers, Detectors and Associated Equipment*, 798, 172, doi: <https://doi.org/10.1016/j.nima.2015.06.058>
- The Pierre Auger Collaboration, Aab, A., Abreu, P., et al. 2017, *Science*, 357, 1266, doi: [10.1126/science.aan4338](https://doi.org/10.1126/science.aan4338)

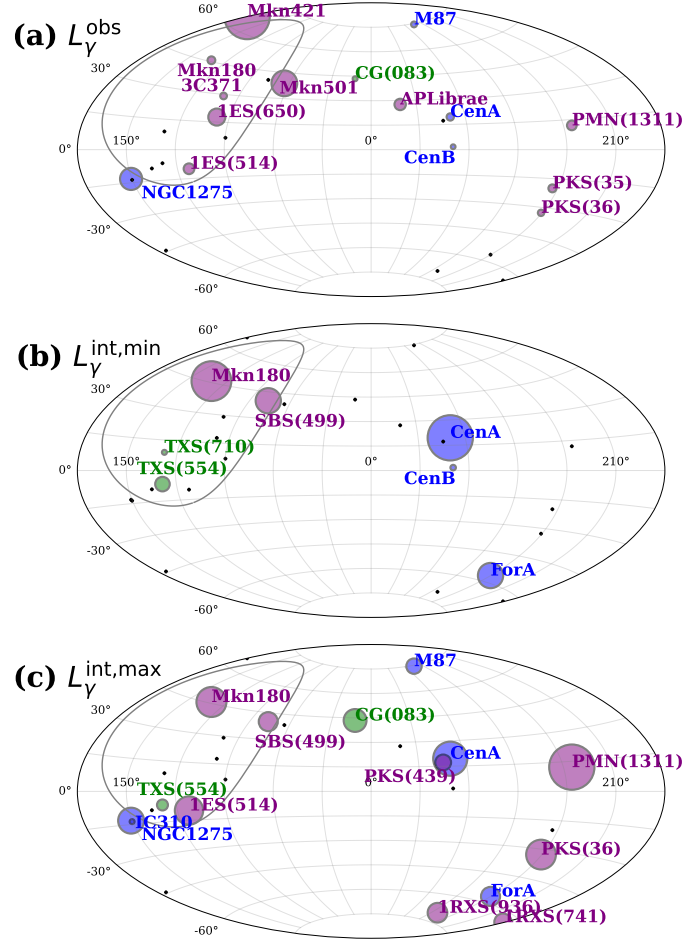
- Turner, R. J., Yates-Jones, P. M., Shabala, S. S., Quici, B., & Stewart, G. S. C. 2022, *Monthly Notices of the Royal Astronomical Society*, 518, 945, doi: [10.1093/mnras/stac2998](https://doi.org/10.1093/mnras/stac2998)
- Verzi, V. 2020, *PoS, ICRC2019*, 450, doi: [10.22323/1.358.0450](https://doi.org/10.22323/1.358.0450)
- Wykes, S., Hardcastle, M. J., & Croston, J. H. 2015, *Monthly Notices of the Royal Astronomical Society*, 454, 3277, doi: [10.1093/mnras/stv2187](https://doi.org/10.1093/mnras/stv2187)
- Wykes, S., Intema, H. T., Hardcastle, M. J., et al. 2014, *Monthly Notices of the Royal Astronomical Society*, 442, 2867, doi: [10.1093/mnras/stu1033](https://doi.org/10.1093/mnras/stu1033)
- Ye, X.-H., Zeng, X.-T., Huang, D.-Y., et al. 2023, *Publications of the Astronomical Society of the Pacific*, 135, 014101, doi: [10.1088/1538-3873/acb291](https://doi.org/10.1088/1538-3873/acb291)
- Yushkov, A. 2020, *PoS, ICRC2019*, 482, doi: [10.22323/1.358.0482](https://doi.org/10.22323/1.358.0482)
- Zhang, B. T., & Murase, K. 2023, *Monthly Notices of the Royal Astronomical Society*, 524, 76, doi: [10.1093/mnras/stad1829](https://doi.org/10.1093/mnras/stad1829)
- Zhang, L., Chen, S., Xiao, H., Cai, J., & Fan, J. 2020, *The Astrophysical Journal*, 897, 10, doi: [10.3847/1538-4357/ab9180](https://doi.org/10.3847/1538-4357/ab9180)

Table 1. Relevant data for the AGNs used in the analysis.

AGN	Class	Distance (Mpc)	$F_\gamma$ ( $10^{-12}$ cm $^{-2}$ s $^{-1}$ ) <sup>a</sup>	$\mathcal{D}$	$\mathcal{D}^b$	$\mathcal{D}^{-4} F_\gamma$
Cen A	RG	3.68	1.54	1 (H.E.S.S. Collaboration et al. 2018; Ye et al. 2023)	1.54	0.0012 – 0.31
M 87	RG	16.7	0.98	1.33-5.3 (MAGIC Collaboration et al. 2020a; Ye et al. 2023)	0.48	2.3 × 10 $^{-2}$
Formax A	RG	20.4	0.48	1 (Ye et al. 2023)	0.48	0.0059 – 0.89
Cen B	RG	55.2	0.64	2.3 (Ye et al. 2023)	2.3	(0.041 – 3.2) × 10 $^{-2}$
NGC 1275	RG	78	14.17	2-7 (Aleksić, J. et al. 2014; Ye et al. 2023)	1.8 × 10 $^{-2}$	4.2 × 10 $^{-3}$
IC 310	RG	83.2	0.43	1.9-5.7 (Ahnen, M. L. et al. 2017; Ye et al. 2023)	3.36 (Ye et al. 2023)	(0.0095 – 2.9) × 10 $^{-3}$
TXS(710)=TXS 0149+710	BCU	103	0.44	2.21 (Ye et al. 2023)	12-50 (Abdo et al. 2011a; Zhang et al. 2020)	(0.0082 – 1.8) × 10 $^{-2}$
NGC 1218 (3C 78)	RG	125	0.54	3.36 (Ye et al. 2023)	6-22 (Abdo et al. 2011b; Zhang et al. 2020)	0.16
Mkn 421	BLL	134	59.35	1.2 (Lister et al. 2020)	6.9 × 10 $^{-5}$ – 0.69	4.0 × 10 $^{-5}$ – 0.40
Mkn 501	BLL	152	19.17	-	4.1 × 10 $^{-6}$ – 1.1	2.7 × 10 $^{-4}$ – 2.7
TXS(554)=TXS 0128+554	BCU	163	0.33	-	1.33-30 (Liiodakis et al. 2018; Acciari et al. 2020a)	1.2
CG(083)=CGCG050-083	BCU	179	0.69	-	1.01 (Liiodakis et al. 2018)	1.35 × 10 $^{-6}$
IRXS(741)=IRXSJ022314.6-111741	BLL	183	0.40	-	50 (MAGIC Collaboration et al. 2020b)	0.48
1ES(514)=1ES 2344+514	BLL	197	3.32	1.33-30 (Liiodakis et al. 2018; Acciari et al. 2020a)	0.27 (Liiodakis et al. 2018)	1.6 × 10 $^{-5}$
PMN(1311)=PMN J0816-1311	BLL	200	2.71	-	22 (Hervet, O. et al. 2015)	1.6 × 10 $^{-7}$
Mkn 180	BLL	203	1.74	-	40 (Acciari et al. 2020b)	5.2 × 10 $^{-3}$
1ES(650)=1ES 1959+650	BLL	212	8.43	-	3.98 (Zhang et al. 2020)	3.3 × 10 $^{-5}$ – 0.33
SBS(499)=SBS 1646+499	BLL	213	0.48	-	6.85-20.8 (Ye et al. 2023; HESS Collaboration et al. 2018)	5.1 × 10 $^{-5}$ – 0.51
APLibrae	BLL	217	3.76	-	40 (Acciari et al. 2020b)	(0.11 – 8.2) × 10 $^{-4}$
TXS 0210+515	BLL	219	0.42	-	40 (Acciari et al. 2020b)	2.3 × 10 $^{-7}$
3C 371	BLL	226	1.3	-	-	1.2 × 10 $^{-4}$ – 1.2
PKS(439)=PKS 1349-439	BLL	228	0.33	-	-	-
IRXS(936)=IRXSJ020021.0-410936	BLL	234	0.51	-	-	-
PKS(35)=PKS 0625-35	BLL	239	1.81	6.85-20.8 (Ye et al. 2023; HESS Collaboration et al. 2018)	-	-
1ES 2037+521	BLL	239	0.58	40 (Acciari et al. 2020b)	-	-
PKS(36)=PKS 0521-36	BLL	241	1.17	-	-	-

NOTE—

<sup>a</sup>Flux between 0.01 and 1 TeV from the Fermi 3FHL catalog, taken from Abdal Halim et al. (2024).<sup>b</sup>As considered by Ye et al. (2023) values  $\mathcal{D} < 1$ . are assumed equal to 1.



**Figure 1.** Luminosity weights used as a proxy for the UHECR flux of AGNs. (a) Using the observed  $\gamma$ -ray flux. (b) Intrinsic  $\gamma$ -ray luminosity estimated as  $L_{\gamma}^{\text{int,min}} = D_{\text{max}}^{-4} L_{\gamma}$ . (c) Intrinsic  $\gamma$ -ray luminosity estimated as  $L_{\gamma}^{\text{int,max}} = D_{\text{min}}^{-4} L_{\gamma}$ . The circle size is linearly proportional to the contribution of each source. Sources with a contribution above  $10^{-2}$  of the maximum contribution are shown as circles (blue = RG, green = BCU, purple = BLL). The other sources are represented by black diamonds.

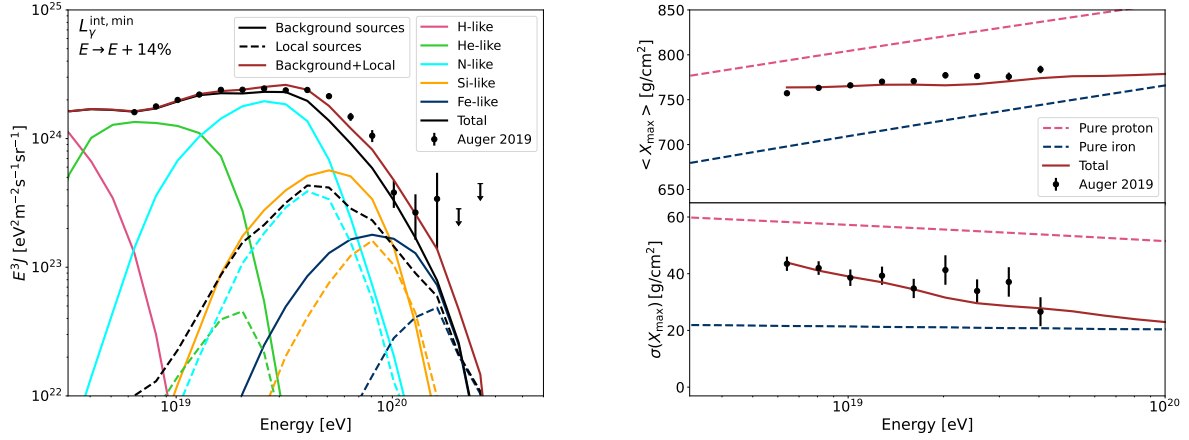


**Figure 2.** Spectrum (left) and first two moments of the  $X_{\max}$  distribution (right) for the best-fit case scenario using  $L_{\gamma}^{\text{int, min}}$  as a proxy. The full and dashed lines in the left panel show the contribution of background and local sources, respectively. The different masses arriving on Earth are grouped into H-like ( $A = 1$ ), He-like ( $2 \leq A \leq 4$ ), N-like ( $5 \leq A \leq 22$ ), Si-like ( $23 \leq A \leq 38$ ), and Fe-like ( $39 \leq A \leq 56$ ) and are represented by the different colors. The dashed lines on the right panel show the expectations for an extreme pure composition scenario. The best-fit parameters are  $\Gamma = -2.2$ ,  $R_{\max} = 10^{18.14}$  V,  $F_i = (2.2 \times 10^{-4}, 0.13, 0.79, 0.08, 2.2 \times 10^{-4})$ , and  $\alpha = 18.025\%$ . A systematic shift of  $E \rightarrow E + 14\%$  is preferred.

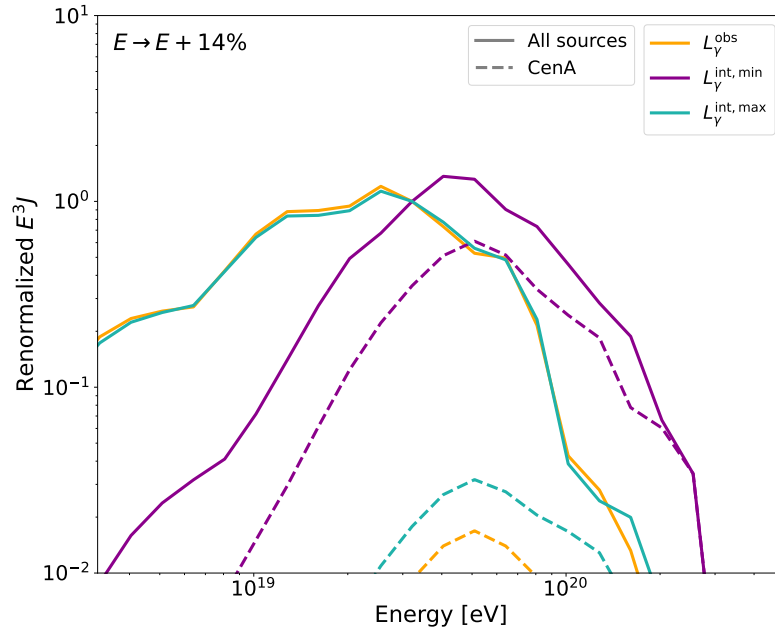


**Figure 3.** Contribution of local sources to the spectrum for the best fit of each  $\gamma$ -ray flux proxy. The spectra are normalized to their value at  $E = 10^{19.5}$  eV in order to ease the comparison of their main structure. The result for each proxy is shown as a different color and the individual contribution of CenA, the closest source considered, is shown by the dashed lines.

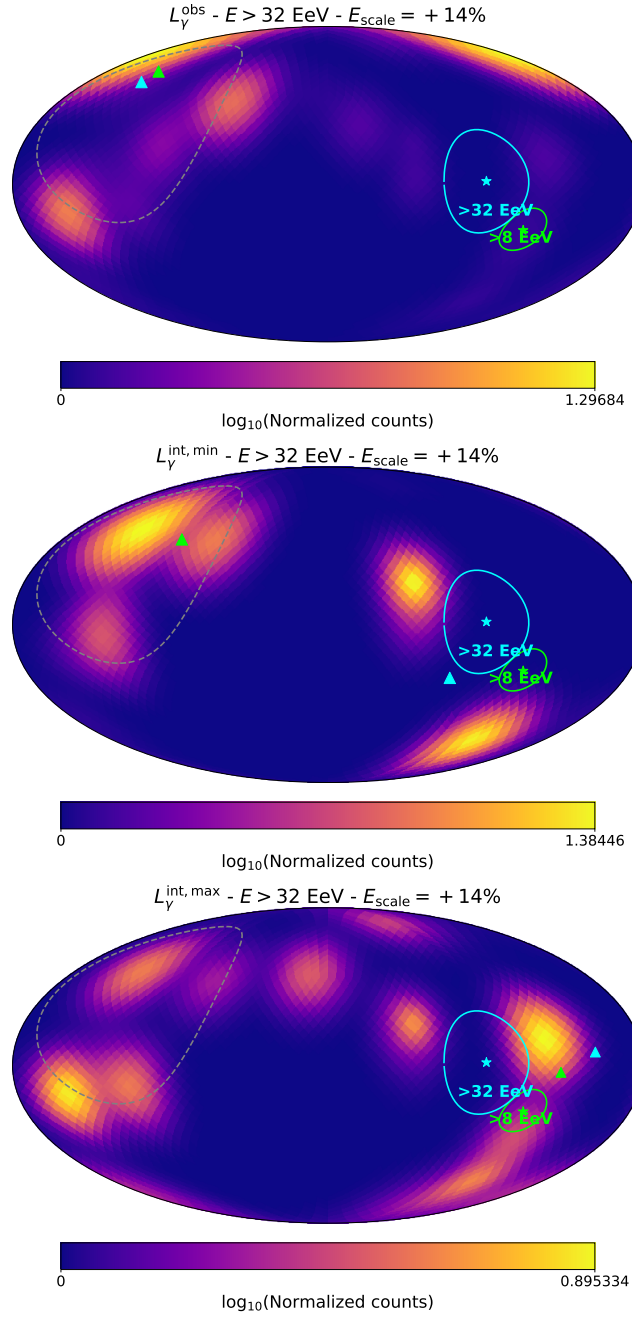


**Figure 4.** Arrival direction maps for  $E > 32 \text{ eV}$ . Each panel shows the results from the best-fit scenario considering each of the  $\gamma$ -ray proxies. The counts are normalized to the bin with the fewest counts, i.e., regions that have negligible contribution from local sources. The lime and cyan stars and contours show the dipole measured by the Pierre Auger Observatory for  $E > 8 \text{ eV}$  and  $E > 32 \text{ eV}$ , while the triangles show the obtained dipoles in the Auger field of view for our scenarios for the same energies. The dashed gray contour shows Auger’s field of view considering events with zenith angles smaller than  $80^\circ$ . A blurring following a Von Mises-Fisher with  $\Delta_0 = 5^\circ$  was used for the local sources.